

# Photonic Topological Insulating Phase Induced Solely by Gain and Loss

Kenta Takata and Masaya Notomi

NTT Nanophotonics Center, NTT Corporation, 3-1 Morinosato-Wakamiya, Atsugi 243-0198, Kanagawa, Japan and  
NTT Basic Research Laboratories, NTT Corporation,  
3-1 Morinosato-Wakamiya, Atsugi 243-0198, Kanagawa, Japan

(Dated: December 14, 2024)

We reveal a one-dimensional bulk topological insulating phase induced solely by gain and loss control in non-Hermitian optical lattices. The system comprises units of four homogeneously coupled cavities, where successive two have loss, the others experience gain and they are balanced under two magnitudes. The gain and loss parts are effectively decoupled and hence *dimerized*, leading to both a bulk bandgap and midgap topologically protected edge states in finite systems. Topological transitions, interface states and stable bound states with global  $\mathcal{PT}$  symmetry are all achievable by controlled pumping in the system.

Controlling the optical properties with external signals has been a major destination in photonics research [1], and it is largely associated with tailoring the refractive index. It has recently been revealed that the imaginary part of the refractive index, namely optical gain and loss, can lead to a rich variety of phenomena other than just tuning the optical intensity. Parity-time ( $\mathcal{PT}$ ) symmetry [2, 3], the key concept proposed by Bender and coworkers, was originally developed for obtaining real spectra of quantum systems even with non-Hermitian components. Its analogy in optics [4, 5] corresponds to complex refractive indices with symmetric real parts and antisymmetric imaginary parts in space, i.e.  $n(\mathbf{r}) = n^*(-\mathbf{r})$ . Such a system can show an exotic exceptional point [6] where its eigenfrequency detuning sharply changes from real to imaginary values [7, 8] (spontaneous  $\mathcal{PT}$  symmetry breaking). There are many interesting phenomena related to  $\mathcal{PT}$  symmetry including power oscillation [4, 9], double refraction [4, 10], Bloch oscillation [11, 12], mode-locking [13], coherent absorption [14–16], fast light [10, 17, 18], and unidirectional reflectivity [19–21]. Furthermore, nonlinearity-induced optical isolation [22, 23], single-mode lasing [24, 25], and beam steering [26] have been achieved under controlled pumping.

To widen the scope of non-Hermitian optics [27, 28], there has also been growing interest in incorporating topological features to photonic systems with gain and loss. While Hermitian photonic topological phases [29–31] are based on celebrated discoveries in condensed matter physics such as the quantum Hall effect [32, 33] and topological insulators [34, 35], non-Hermitian topological optics originates from the theoretical question as to whether or not topological quantum states exist in non-Hermitian systems [36–40]. For photonics based on classical electromagnetic waves, however, it has been clarified that there exist topological states that are robust to certain types of perturbation, even when their eigenvalues are not real [41]. Researchers applied Su-Schrieffer-Heeger (SSH) photonic lattices [42] with judicious inclusion of relevant loss and experimentally confirmed their topological interface states [43] and topological transition [44]. Moreover, a topological protection by global  $\mathcal{PT}$  symmetry was also observed in a waveguide array

[45]. It has been recently shown that even the lasing of photonic topological edge states is feasible [46–49].

Then, another question may arise. *Is it possible to create a topologically-nontrivial insulating phase solely from gain and loss control?* In previous studies of non-Hermitian optics, the emergence of nontrivial topologies was attributed to their Hermitian factors, namely the magneto-optic effect [49] and the host system structures such as SSH lattices [50], Aubry-André lattices [51], lattices with second-nearest-neighbor coupling [52] and strong coupling [53], and some SU(1,1) and SO(3,2) models [37]. Even though such systems are armed with non-Hermiticity, they just take over original Hermitian topological features. Moreover, the literature has shown that gain and loss in conventional non-Hermitian systems [27, 28, 54] only close the frequency bandgap. Thus, they were considered to destroy topological insulating phases. In contrast, our aim is to generate a complete topological bandgap solely by adding static gain and loss to a topologically trivial structure. Then, the achieved topological features, with a well-defined topological number, should originate purely from non-Hermitian factors. Here, the gain and loss are readily tunable by external injection current with independent electric channels or optical pumping with spatial light modulation in photonic devices, such as microring and polariton laser arrays [46–48], surface emitting lasers [26] and photonic crystal lasers [18]. We will hence have full manipulability over the topological features in optical circuits, such as a topological transition, and the number and position of topological states, simply by changing the gain and loss. This is in a stark contrast to topological optical systems whose features are predetermined by fabrication.

Here, we show theoretically a photonic lattice with the gain- and loss-induced reconfigurable topological insulating phase. We consider the unit cells of four homogeneously coupled resonators, with loss introduced into two successive cavities and gain introduced into the other two. This is a minimum non-Hermitian extension for systems with two-cavity units (covering the SSH model), namely doubling the number of cavities as room for the introduction of gain and loss. Our system then forms a pair of dimers by the effective decoupling between cavi-

ties with gain and loss. This can result in a bulk bandgap, topological transition and edge states for a wide range of parameters. Topological interface states can also be formed on the boundary between the nontrivial and trivial lattices. These properties are achievable also in a system under an arbitrary offset loss or gain factor on every element (“loss or gain bias”). Our scheme will hence provide broad opportunities for its experimental demonstration and applications. The system is unique in terms of non-Hermiticity-induced midgap edge states with the standard topological protection by their isolation from bulk states, compared to defect and edge states in gapless systems [37, 55–57].

*Theoretical model.*— The considered system has periods of four single-mode cavities with uniform couplings  $\kappa$ , as shown in Fig. 1 (a). Without any gain or loss, the bulk cavity array does not exhibit a bandgap [Fig. 1 (b)]. We introduce an on-site imaginary potential profile  $(ig_1, -ig_2, -ig_1, ig_2)$  for the four cavities, with their positive and negative coefficients meaning gain and loss, respectively. Here, we assume that  $\kappa$ ,  $g_1$  and  $g_2$  are sufficiently small compared to the cavities’ resonant frequency  $\omega_0$  and their Q-factors are high, so that we can safely neglect the effect of the imaginary index profile and radiation loss on the coupling coefficient, as expected in various semiconductor laser systems [18, 22, 23, 25, 26, 46–48]. The real index modulation by the Kramers-Kronig relations will also be restricted or cancelled by tuning the cavities thermally [58] and placing a loss or gain bias  $i\gamma$  to every cavity [59], which do not change the properties of the system except for  $i\gamma$  added to the eigenvalues. Within the linear analysis, the coupled mode equation describing the base system is equivalent to the Schrödinger equation  $i\partial_t |\Psi\rangle = \hat{H} |\Psi\rangle$ , where  $|\Psi\rangle = (\{\Psi_n\})^T$  is the vector of the slowly-varying complex cavity-mode amplitudes ( $n$ : cavity index) and  $\hat{H}$  is a tight-binding lattice Hamiltonian. Considering the Bloch theorem and a dynamical factor  $e^{-i\omega t}$ , the analysis is reduced to an eigenvalue problem for the four-component eigenvector  $|\psi_B\rangle$  under the Bloch Hamiltonian  $\hat{H}(k)$ ,

$$\hat{H}(k) = \begin{pmatrix} ig_1 & \kappa & 0 & \kappa e^{-ika} \\ \kappa & -ig_2 & \kappa & 0 \\ 0 & \kappa & -ig_1 & \kappa \\ \kappa e^{ika} & 0 & \kappa & ig_2 \end{pmatrix}, \quad (1)$$

where  $a$  is the spatial interval between four-cavity units and  $k$  is the Bloch wavenumber. The eigenfrequency detuning  $\omega(k)$  with reference to  $\omega_0$  is given by,

$$\omega(k) = \pm \frac{1}{\sqrt{2}} \sqrt{A \pm \sqrt{A^2 - B^2 - 16\kappa^2 \sin^2 \frac{ka}{2}}}, \quad (2)$$

where  $A = 4\kappa^2 - g_1^2 - g_2^2$  and  $B = 2g_1g_2$ . We also find analytic forms of  $|\psi_{B,s}\rangle$  ( $s$ : eigenstate index), although they are too complicated to be given here. In the following analysis, the gain and loss are measured with respect to the cavity coupling, i.e.  $\kappa = 1$ . We also focus on the

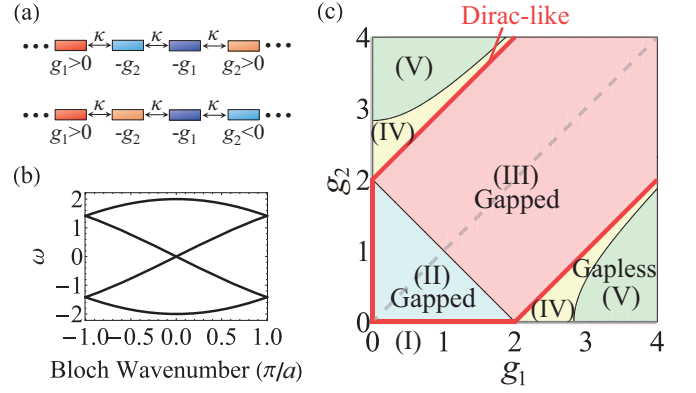


FIG. 1. (Color online) (a) Schematic of considered system. Upper and lower lattices for  $g_2 > 0$  and  $g_2 < 0$  are topologically nontrivial and trivial, respectively. (b) Folded cosinusoidal band structure for  $g_1 = g_2 = 0$ . (c) Phase diagram for the system band structure.  $\kappa = 1$ ,  $g_1, g_2 \geq 0$ . Thick lines: condition for Dirac-like dispersion in  $\text{Re} \omega(k)$ .

case where  $g_1 > 0$  and  $g_1 \geq |g_2|$  for studying the bulk properties, because the spatial and/or time reversal can map the system with this condition to that with the other parameter range. Note that when  $g_1 = g_2 = 0$ , the system has a four-fold cosinusoidal band structure and two degenerate states with  $\omega(0) = 0$ , because of the reduced first Brillouin zone [Fig. 1 (b)].

The system band structure is classified into five patterns via the value of the inside of the double radical sign of Eq. (2) for  $k = 0$  [Fig. 1 (c)]. With  $g_1, g_2 \geq 0$  for simplicity, the divided phase regions are, (I)  $B = 0$ , (II)  $A + B > 0$ ,  $A - B \geq 0$ , (III)  $A + B > 0$ ,  $A - B < 0$ , (IV)  $A + B \leq 0$ ,  $A^2 - B^2 - 16\kappa^2 < 0$  and (V)  $A^2 - B^2 - 16\kappa^2 \geq 0$ . As shown later, the systems in phase (II) and (III) have complete frequency bandgaps and those in phase (I), (IV) and (V) are gapless. We consider phase (I), (II) and (III) here and mention (IV) and (V) elsewhere [60]. Note that the phase boundaries are symmetric to  $g_1 = g_2$  in Fig. 1 (c), and the diagram for  $g_2 < 0$  is obtained by the mirror inversion of Fig. 1 (c) with regard to  $g_2 = 0$ .

In Eq. (2), we see that  $\omega(k)$  is real as long as  $A > 0$  and  $A^2 - B^2 - 16\kappa^2 \sin^2(ka/2) > 0$ . Such real eigenvalues are expected because the bulk Hamiltonian  $\hat{H}(k)$  has pseudo-Hermiticity [61], i.e.  $\hat{S}(k)\hat{H}(k)\hat{S}(k) = \hat{H}^\dagger(k)$ . Here, the  $k$ -dependent linear operator  $\hat{S}(k) = \hat{S}(k)^{-1} = \hat{\sigma}_x \otimes (\cos \frac{k}{2})\hat{I}_2 + \hat{\sigma}_y \otimes (\sin \frac{k}{2})\hat{I}_2$  means a half-period translation.  $\hat{\sigma}_{x,y,z}$  are Pauli matrices and  $\hat{I}_2$  is the  $2 \times 2$  identity matrix. The pseudo-Hermiticity guarantees an associated antilinear symmetry [62]. Although the system does not respect  $\mathcal{PT}$  symmetry, the bulk antilinear symmetry can instead cancel its gain and loss and give at least partially real spectra, i.e.  $\text{Im} \omega(k) = 0$ . Meanwhile, the antilinear operation to which  $\hat{H}(k)$  shows the invariance is implicit due to its eigenvector dependence.

We point out that Eq. (2) satisfies a pseudo-anti-Hermiticity [36, 37, 60],  $\hat{H}(k) = -\hat{\eta}\hat{H}^\dagger(k)\hat{\eta}$ , where  $\hat{\eta} =$

$\hat{I}_2 \otimes \hat{\sigma}_z = \text{diag}(1, -1, 1, -1)$  and  $\hat{\eta}^{-1} = \hat{\eta}^\dagger = \hat{\eta}$  in our model. This symmetry can lead to a nontrivial topology via ensured pairs of eigenfrequencies,  $\omega(k)$  and  $-\omega^*(k)$ . Since  $\hat{\eta}$  is local (diagonal), the topological protection by the symmetry covers all the parameters in our system.

**Bulk properties.**— In the system, a topological bandgap can be opened and closed by the two magnitudes of balanced gain and loss. Figure 2 shows the real and imaginary band structures and eigenmode distributions of the system with different  $g_1$  and  $g_2$  values. When  $g_1 \neq 0$  and  $g_2 = 0$  [phase (I)], the eigenstates around  $\omega(0) = 0$  for  $A > 0$  have a Dirac-like dispersion [Fig. 2 (a)] with cancelled net gain and loss:  $\text{Im}\omega(k) = 0$  [Fig. 2 (b)], reflecting the antilinear symmetry. This gapless band structure is because  $B = 0$  in Eq. (2). It indicates that the topological transition point of the Hermitian SSH model, namely  $\kappa_1 = \kappa_2$  for its two generally different couplings  $\kappa_1$  and  $\kappa_2$ , is extended to the non-Hermitian regime along with  $g_1 \neq 0$ ,  $g_2 = 0$  and  $g_1 = 0$ ,  $g_2 \neq 0$  in our model. The condition of  $(g_1, g_2)$  for the emergence of the relevant Dirac cone also includes the boundary between phase (II) and (III) [highlighted in Fig. 1 (c)]. The band structure also has two exceptional points corresponding to the spontaneous antilinear symmetry breaking. The intensity distributions for the eigenstates  $|\psi_{B,s}\rangle$  [Fig. 2 (c)] show that the fields are evenly distributed in the gain and loss cavities ( $n = 1$  and  $3$ ) before this transition ( $k = 0.05\pi/a$ ), while the eigenmodes with the broken symmetry ( $k = 0.95\pi/a$ ) exhibit the localization at either of them, resulting in complex  $\omega(k)$ .

A bandgap opens for both finite  $g_1$  and  $g_2$  under phase (II) due to  $B^2 > 0$  [ $|g_2| \leq 2\kappa - g_1$ , Fig. 2 (c)], while the real eigenvalues remain around the split band center [Fig. 2 (d)]. Here, the effective couplings between gain and loss cavities become *weaker* than that between both gain cavities and that between both loss cavities [60], as deduced from the mode localization by  $\mathcal{PT}$  symmetry breaking [7, 8, 27, 28]. This results in the dimerization of the successive cavities with gain and those with loss, and it essentially needs at least four cavities in the unit cell. The mode patterns for the gapped phases confirm this non-Hermitian effect. All the eigenmodes for phase (II) inside the remaining exceptional points spread over the whole unit cell, cancelling the net gain and loss for real  $\omega(k)$  [ $k = 0.05\pi/a$ , Fig. 2 (f)]. After the symmetry breaking, however, they eventually turn into couples of states with localization at the gain dimer ( $n = 1, 4$ ) and loss dimer ( $n = 2, 3$ ) for complex  $\omega(k)$  ( $k = 0.95\pi/a$ ). This feature is clearly distinct from the case of phase (I). For phase (III),  $|g_2| > 2\kappa - g_1$ , the complete antilinear symmetry breaking makes the pairs of upper and lower real bands overlap and hence gives the split imaginary bands [Fig. 2 (g), (h)]. Thus, only the dimerized eigenstates are allowed all over the Brillouin zone [Fig. 2 (i)]. These data clarify that the non-Hermitian factors in our system contribute to the dimerization. We emphasize that reversing the signs of  $g_1$  and  $g_2$  do not affect the band structure as seen in Eq. (2), while a

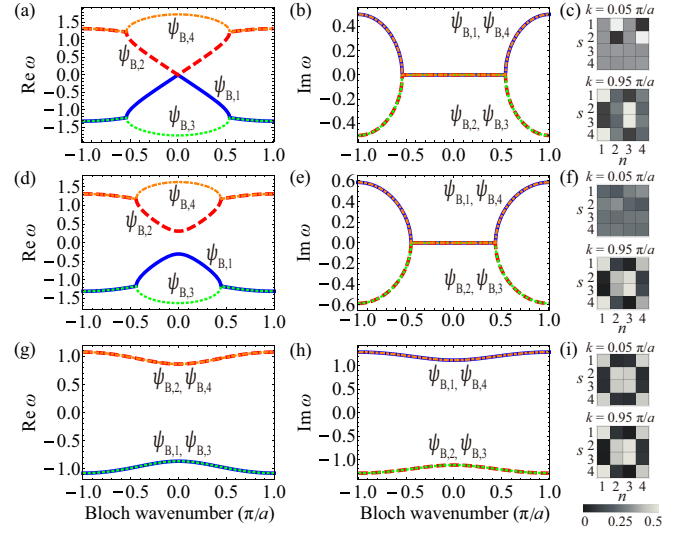


FIG. 2. (Color online) Band structures and mode patterns of system for different gain and loss profiles.  $\kappa = 1$ . (a)  $\text{Re}\omega(k)$ , (b)  $\text{Im}\omega(k)$  and (c)  $|\psi_{B,s,n}|^2 / \langle\psi_{B,s}|\psi_{B,s}\rangle$  for  $g_1 = 1$ ,  $g_2 = 0$ . (d)  $\text{Re}\omega(k)$ , (e)  $\text{Im}\omega(k)$  and (f)  $|\psi_{B,s,n}|^2 / \langle\psi_{B,s}|\psi_{B,s}\rangle$  for  $g_1 = 1$ ,  $g_2 = 0.5$ . (g)  $\text{Re}\omega(k)$ , (h)  $\text{Im}\omega(k)$  and (i)  $|\psi_{B,s,n}|^2 / \langle\psi_{B,s}|\psi_{B,s}\rangle$  for  $g_1 = 2$ ,  $g_2 = 1$ .  $s$  and  $n$ : eigenstate and cavity indices.

topological transition between systems with  $g_2 > 0$  and  $g_2 < 0$  is expected at the Dirac-type gap closing. In addition, the eigenstates in phase (III) are not degenerate in terms of complex  $\omega(k)$ , thus a topological invariance is computable there. Note also that the bandgap broadens continuously as  $(g_1, g_2)$  gets toward the inside of phase (II) and (III) from their boundaries [60].

To clarify possible photonic topologies in our system, we introduce the normalized global Berry phase [63] in  $k$  space. The topological number  $W$  has to take account of the fact that the Zak phase [64] of each band is not discretized because of the degeneracy at the exceptional points and non-Hermitian factors.  $W = \sum_s \frac{i}{4\pi} \oint dk \langle\langle\psi_{B,s}|\partial_k|\psi_{B,s}\rangle\rangle$  denotes the topological feature of the entire system by tracing the single-parameter non-Abelian Berry phase matrix [65] on a biorthonormal basis [66]. Here,  $s = 1, \dots, 4$  is the band index, and  $|\psi_{B,s}\rangle$  the left eigenstate that forms a duality with  $|\psi_{B,s}\rangle$ , namely  $\hat{\mathcal{H}}(k)|\psi_{B,s}\rangle = \omega(k)|\psi_{B,s}\rangle$  and  $\hat{\mathcal{H}}^\dagger(k)|\psi_{B,s}\rangle = \omega^*(k)|\psi_{B,s}\rangle$ . The biorthonormal basis ( $\{|\psi_{B,s}\rangle\}$ ,  $\{|\psi_{B,s}\rangle\}$ ) enables the normalization  $\langle\langle\psi_{B,s}|\psi_{B,t}\rangle\rangle = \delta_{s,t}$  and the extraction of pure phase factors of non-Hermitian eigenvectors.  $W$  also reflects the  $4\pi$  periodicity of the eigenvectors [52, 60]. We notice that when in phase (II), each exceptional point switches the pairing of the dual analytic  $|\psi_{B,s}\rangle$  and  $|\psi_{B,s}\rangle$  due to the emergence of finite  $\text{Im}[\omega(k)]$ . With this point taken into account, we have obtained integer values of  $W = 1$  for  $g_2 > 0$  and  $W = 0$  for  $g_2 < 0$  in phases (II) and (III), where the system holds the bandgap in  $\text{Re}\omega(k)$  [60]. It clearly shows the topological transi-

tion controlled by gain and loss between the two conditions in Fig. 1 (a). The nontrivial bulk photonic topology, expected by our pseudo-anti-Hermiticity and non-Hermiticity-based bandgap opening, has hence been confirmed. Note that  $W$  for the other parameter regions is out of the scope of this paper, because standard topological numbers are basically undefined for completely gapless conditions. Moreover, implicit degeneracy and divergence of the eigenvectors there make the computation difficult.

*Edge states.*— We can clearly discuss the origin of the topological edge states with  $\text{Re}\omega = 0$ , in terms of a particle-hole symmetry [67] equivalent to the pseudo-anti-Hermiticity in our finite lattice model. Because the lattice Hamiltonian  $\hat{\mathcal{H}}$  with a finite number of cavities and the open boundary condition is a symmetric matrix ( $\hat{\mathcal{H}} = \hat{\mathcal{H}}^T$ ), the global pseudo-anti-Hermiticity in our finite system,  $\hat{\mathcal{H}} = -\hat{\eta}'\hat{\mathcal{H}}^\dagger\hat{\eta}'$ , easily reduces to a particle-hole symmetry  $-\hat{\mathcal{H}} = \hat{\eta}'\hat{\mathcal{H}}^*\hat{\eta}'$ . Here,  $\hat{\eta}' = \text{diag}(1, -1, 1, -1, \dots, 1, -1, 1, -1)$  is again a local operator,  $\hat{\eta}'^{-1} = \hat{\eta}'^\dagger = \hat{\eta}'$  and  $\hat{\mathcal{H}}^*$  is the complex conjugation of  $\hat{\mathcal{H}}$ . It indicates that the number of states with  $\text{Re}\omega = 0$  at each edge can change only by two [68, 69]. Thus, a single isolated edge state with  $\text{Re}\omega = 0$  on each side, based on  $(1, 0, 0, \dots, 0)^T$  and  $(0, \dots, 0, 0, 1)^T$  in the system for  $g_1 = g_2 = 0$ , is topologically protected by this symmetry under proper dimerization conditions [70]. Figure 3 confirms the existence of topological edge states in systems with 40 cavities for  $g_1 > 0, g_2 > 0$ . Here, there is relatively weaker effective coupling between gain and loss cavities at both edges [Fig. 3 (a)], which is consistent with the edge-state generation condition in the Hermitian SSH model [42, 50]. Displayed eigenfrequencies show a pair of midgap states for both phase (II) [Fig. 3 (b)] and (III) [Fig. 3 (d)]. Each eigenmode with  $\text{Re}\omega = 0$  is localized at the left or right edge of the system and has  $\text{Im}\omega > 0$  mainly because of the imaginary potential of the relevant edge cavity. Here, a noteworthy difference of the above conditions is whether the localization is unit-based [phase (II), Fig. 3 (c)] or cavity-based [phase (III), Fig. 3 (e)], reflecting whether the bulk eigenstates with  $k = 0$  have  $\text{Im}\omega = 0$  (*exact* phase) or  $\text{Im}\omega \neq 0$  (*broken* phase). We can also obtain topological edge modes with  $\text{Re}\omega = 0$  when each edge is terminated by a loss cavity ( $g_1 < 0, g_2 < 0$ ). However, such states disappear if the unit cell has a cavity with gain on one side and a cavity with loss on the other ( $g_1 g_2 < 0$ ), as indicated by  $W = 0$ . We found an exceptional case of  $g_1 = g_2$  and striking robustness of the edge states to disorder [60].

*Interface states.*— As applications of the controllable photonic topological insulating phases, we present two interface states based on our lattices. One involves direct butting of topologically nontrivial and trivial lattices, forming an effective “long-long defect” [71] at the boundary [Fig. 4 (a)]. Here, the eigenfrequencies of a system in phase (II) exhibit two states with  $\text{Re}\omega = 0$ , while they have relatively large difference in  $\text{Im}\omega$  [Fig. 4 (b)], compared with Fig. 3 (b). Their intensity distributions

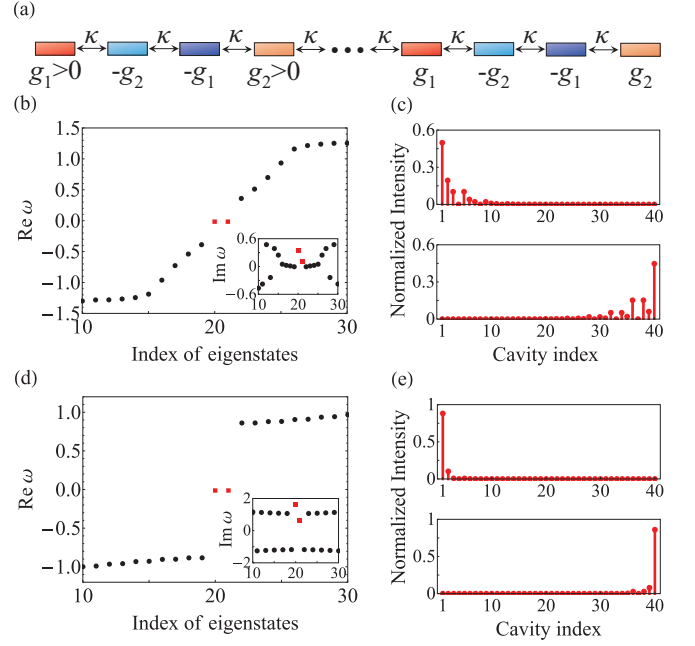


FIG. 3. (Color online) (a) Illustration of a finite non-Hermitian-dimerized topological lattice. (b), (d) Sorted and selected real eigenvalues for a forty-cavity system. Insets: corresponding imaginary eigenvalues. Squares: the topological edge states. (c), (e) Intensity distributions for the topological edge states. (b), (c)  $g_1 = 1, g_2 = 0.5$ . (d), (e)  $g_1 = 2, g_2 = 1$ .

indicate topological edge and interface states with localization at left ( $n = 1$ ) and right ( $n = 20$ ) sides of the non-trivial lattice [Fig. 4 (c)]. Both states are topologically protected because the whole system respects the particle-hole symmetry.  $\text{Im}\omega \sim 0.06$  of the interface state is small but does not vanish, because the finite lattice does not have any global antilinear symmetry. However, we emphasize that an imaginary potential bias  $i\gamma$  can be introduced to compensate for the net gain and loss of the topological states. Including the tunability of  $g_1$  and  $g_2$ , we will be able to stabilize and even oscillate these states with their position and number controlled.

To achieve a topological state fundamentally with  $\text{Im}\omega = 0$ , we place a cavity without gain or loss sandwiched between two 20-cavity lattices with different sequences of two-magnitude gain and loss, so that the whole lattice respects the global  $\mathcal{PT}$  symmetry [45] [Fig. 4 (d)]. Here, the center vacant cavity and left parts can be considered a defective topological lattice, thus a bound state with  $\text{Re}\omega = \text{Im}\omega = 0$  is formed [Fig. 4 (e)]. Its mode profile shows localization at the vacant cavity [ $n = 21$  in Fig. 4 (f)]. Such a bound state is preserved under the combination of the pseudo-anti-Hermiticity and global  $\mathcal{PT}$  symmetry, as shown in Ref. 45.

We have shown the unambiguous answer that the gain and loss can induce the topological insulating phase and control the topological transition, starting from the simple gapless resonator array with the identical couplings. Our model is also valid for coupled waveguides



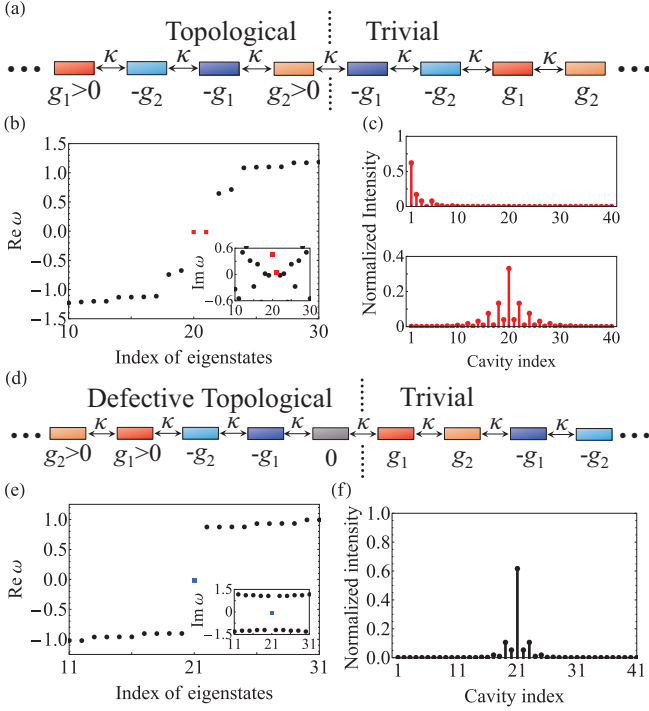


FIG. 4. (Color online) (a) Interface between topologically nontrivial (left) and trivial (right) lattices, each of which has 20 cavities. (b) Sorted and selected  $\text{Re } \omega$ . Inset: corresponding  $\text{Im } \omega$ . Left and right squares: eigenvalues for the edge and interface states. (c) Intensity profiles for the topological edge (upper) and interface (lower) modes.  $g_1 = 1, g_2 = 0.5$ . (d) A system forming a topological bound state based on the global  $\mathcal{PT}$  symmetry, which comprises a single vacant cavity and proposed trivial lattices with 20 cavities on both sides. (e) Selected  $\text{Re } \omega$  and  $\text{Im } \omega$  (inset). Square: the topological bound state with  $\text{Re } \omega = \text{Im } \omega = 0$ . (f) Intensity profile for the bound state.  $g_1 = 2, g_2 = 1$ .

[44, 45] and experimentally feasible by modifying the existing laser arrays with controlled optical pumping [46–48]. Moreover, it can be explored as an extension of  $\mathcal{PT}$ -symmetric setups in not only photonics [10, 18, 22–26, 43] but also phononics [72–74], and circuit electronics [75, 76]. This scheme would pave the way for various possibilities of non-Hermitian topological photonics, such as reconfigurable topological lasing states, purely non-Hermiticity-based topological pumping [41], topological superstructures [77] and Floquet topological systems [40, 78], and variations of dynamically encircling exceptional points for asymmetric mode control [79, 80]. Extending the topological controllability to two-dimensional systems is another important direction.

#### ACKNOWLEDGMENTS

We thank Hiroshi Yamaguchi, Kensuke Inaba and Koji Muraki for fruitful discussions. This work was supported by JST through CREST program (No. JPMJCR15N4).

#### Appendix A: Gapless Phases

We have presented a phase diagram for the band structure of the considered system [Fig. 1 (c) in the main text]. Here, we discuss the bulk properties of the systems under phase (IV) and (V), which exhibit gapless band structures. The system in phase (II) and (III) has a complete bandgap in  $\text{Re } \omega(k)$  ( $k$ : Bloch wavenumber). However, the gap closes at the boundary  $|g_2| = g_1 - 2\kappa$ , and this results in linear dispersion around the degeneracy as phase (I) ( $g_1, g_2$ : magnitudes of gain and loss,  $\kappa$ : cavity coupling rate). The band structure in phase (IV) hence has a flat region in its real part with  $\text{Re } \omega(k) = 0$  around  $k = 0$  [Fig. 5 (a)]. Here, there exist two bifurcation points [exceptional points (EPs)] in  $\text{Re } \omega(k)$ . The corresponding curved imaginary bands around  $k = 0$  coalesce in pairs at the EPs [Fig. 5 (b)], forming two “exceptional rings” [81] in both  $\text{Im } \omega(k) > 0$  and  $\text{Im } \omega(k) < 0$ . Such rings are lost in phase (V); the overlapped flat real bands extend [Fig. 5 (c)], and all the imaginary band curves are split [Fig. 5 (d)] over the entire first Brillouin zone. We notice that two eigenstates in phase (IV) [Fig. 5 (b)] have jumps in  $\text{Im } \omega(k)$  at EPs. This is because  $\omega(k)$  has double radical signs, and such jumps are caused by non-Hermiticity.

#### Appendix B: Bandgap

Figure 6 show the width of the system bandgap  $\Delta$  for  $\text{Re } \omega(k)$  depending on the gain and loss. Here, the bandgap in our model is determined by the eigenfrequencies at  $k = 0$ . Fig. 6 (a) presents the dependence of the two-dimensional parameter space ( $g_1 > 0, g_2 > 0$ ).  $\Delta$  enlarges continuously as  $g_1$  and  $g_2$  increase in phase (II). In contrast, the gap in phase (III) has the maximum ( $\Delta = 2$ ) along with  $g_1 = g_2$  and falls down to zero abruptly at the boundary between phase (III) and (IV), by the rise in either  $g_1$  or  $g_2$ . For a cross-section view, Fig. 6 (b), both  $g_1$  and  $g_2$  are varied so that they satisfy the relation  $g_2 = g_1 - 1$  ( $g_1 \geq 1$ ). When  $g_2$  increases from zero, the parameters ( $g_1, g_2$ ) move in parallel with the boundary between phase (III) and (IV), away from (1, 0) on phase (I). As a result, the bandgap in phase (II) approaches sharply the value  $\sqrt{2(4\kappa^2 - g_1^2 - g_2^2)} = \sqrt{3}$  ( $g_1 = 1.5, g_2 = 0.5$  here), reflecting the complete anti-symmetry breaking at the boundary between phase (II) and (III).  $\Delta$  is then constant in phase (III) ( $g_2 > 0.5$ ) for this linear dependence, meaning that the dimer with gain and that with loss remain decoupled there.

#### Appendix C: Effective Decoupling by Gain and Loss

We can estimate the effective cavity decoupling induced by gain and loss with a simple two-cavity system.

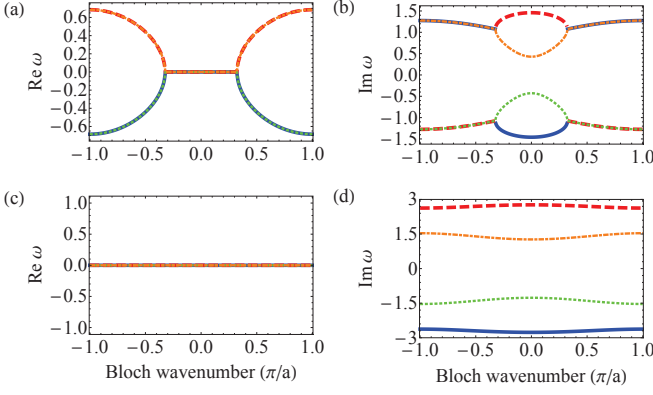


FIG. 5. Real and imaginary band structures of the system in phases (IV) and (V).  $\kappa = 1$ . (a)  $\text{Re } \omega$  and (b)  $\text{Im } \omega$  for  $g_1 = 2.5$  and  $g_2 = 0.25$ , in phase (IV). (c)  $\text{Re } \omega$  and (d)  $\text{Im } \omega$  for  $g_1 = 3.5$  and  $g_2 = 1$ , in phase (V).

We consider the Hamiltonian,

$$\hat{\mathcal{H}}(k) = \begin{pmatrix} i\gamma_1 & \kappa \\ \kappa & i\gamma_2 \end{pmatrix}, \quad (\text{C1})$$

and its eigenvalues  $\lambda = i(\gamma_1 + \gamma_2)/2 \pm \sqrt{\kappa^2 - (\gamma_1 - \gamma_2)^2/4}$ , where  $\gamma_1$  and  $\gamma_2$  are the imaginary potentials of the cavities. By comparing  $\lambda$  with the eigenvalues without any gain and loss,  $\lambda(g_1, g_2 = 0) = \pm\kappa$ , we can understand that the coupling, in terms of the splitting of  $\text{Re } \lambda$ , is effectively reduced from  $\kappa$  to  $\kappa' = \sqrt{\kappa^2 - (\gamma_1 - \gamma_2)^2/4}$ . Thus, it is expected that the local effective coupling decreases depending on the difference between the imaginary potentials of adjacent cavities,  $|\gamma_1 - \gamma_2|$ .

With this supposition, the four-cavity system considered in this work provides two effective couplings,  $\kappa'_1 = \sqrt{\kappa^2 - (g_1 + g_2)^2/4}$  and  $\kappa'_2 = \sqrt{\kappa^2 - (g_1 - g_2)^2/4}$ . Here, we can see that substituting these effective couplings into the bandgap of the Hermitian SSH model [42] reproduces that of our four-cavity model,  $\Delta = \sqrt{2}\sqrt{A - \sqrt{A^2 - B^2}}$ , where  $A = 4\kappa^2 - g_1^2 - g_2^2$  and  $B = 2g_1g_2$ . This implies that the gradient of the system's imaginary potential is relevant to dimerization, as discussed in the main text. This correspondence is because, at the band center that gives the frequency gap, the impact of periodicity is eliminated and the pseudo Hermiticity cancels out the effect of  $\text{Im } \lambda$ . It is noteworthy that the SSH model does not reproduce the band structure of the four-cavity system for  $k \neq 0$ .

#### Appendix D: Topological number

Figure 7 shows the normalized global Berry phase  $W$  for the gapped system in phases (II) and (III), for  $g_2 > 0$  and  $g_2 < 0$ . Here,  $W = 1$  for  $g_2 > 0$  and  $W = 0$  for  $g_2 < 0$  are confirmed with negligible errors, for all the considered values of  $(g_1, g_2)$ . It clearly shows that the

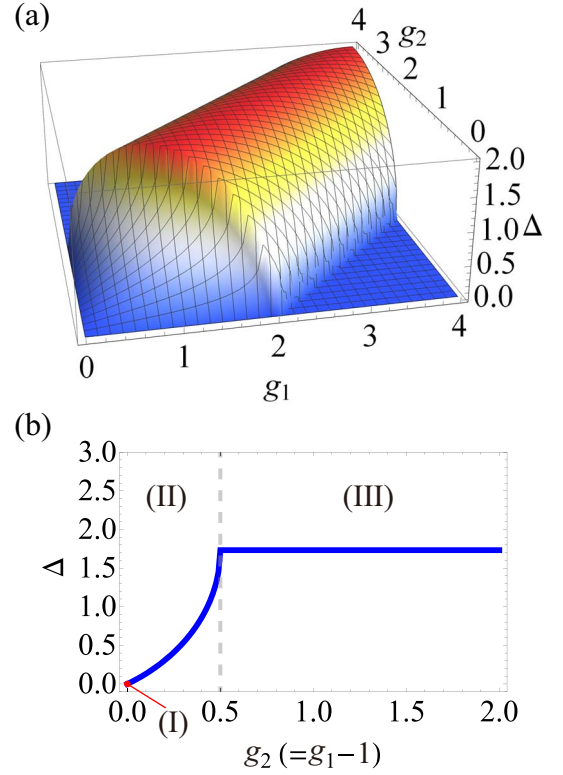


FIG. 6. The system frequency bandgap  $\Delta$  dependent on the gain and loss. (a)  $\Delta$  for the two-dimensional parameter space ( $g_1 > 0, g_2 > 0$ ). (b) A cross-sectional view with  $g_2 = g_1 - 1$  ( $g_1 \geq 1$ ), for phase (I) ( $g_2 = 0$ ), (II) ( $0 < g_2 < 0.5$ ) and (III) ( $g_2 > 0.5$ ).

Non-Hermitian topological transition occurs at the gap closing with  $g_2 = 0$ . In the  $W$  calculation, it is noteworthy that the two EPs encountered with phase (II) are excluded from the integral range, because of the following special properties of EPs. First, pairs of dual states change at EPs [82], as described in the main text. Thus, numerical integration cannot involve an EP when a single left eigenstate  $\langle\langle\psi_{B,s}|$  is considered. Second, it is known that the norm  $\langle\langle\psi_{B,s}|\psi_{B,s}\rangle\rangle$  itself vanishes at EPs (self-orthogonalization) [83]. This makes unable for numerical differentiation algorithms to use the eigenstates exactly at EPs, even under the normalization based on the biorthonormal basis. Note that we took into consideration the combined EP in  $\text{Im } \lambda$  remaining at  $k = 0$  for the boundary between phases (II) and (III). The removed wavenumber ranges are  $[-k_{\text{EP}} - 2\Delta k, -k_{\text{EP}} + 2\Delta k]$  and  $[k_{\text{EP}} - 2\Delta k, k_{\text{EP}} + 2\Delta k]$ , where  $k_{\text{EP}}$  denotes an EP with  $k > 0$ . Fortunately, these widths can be arbitrarily small, depending on the unit wavenumber step  $\Delta k$  in the numerical differential. We found that  $W \rightarrow 1$  for  $g_2 > 0$  and  $W \rightarrow 0$  for  $g_2 < 0$  with  $\Delta k \rightarrow 0$  [Fig. 7 (a)]. Here,  $\Delta k = 10^{-10}$  is used for the computation.  $|\text{Im } W|$  for each  $(g_1, g_2)$  is less than  $2 \times 10^{-16}$  and hence can be said to be numerically zero. Note that the biorthonormality of the eigenstates is guaranteed except for the EPs, because

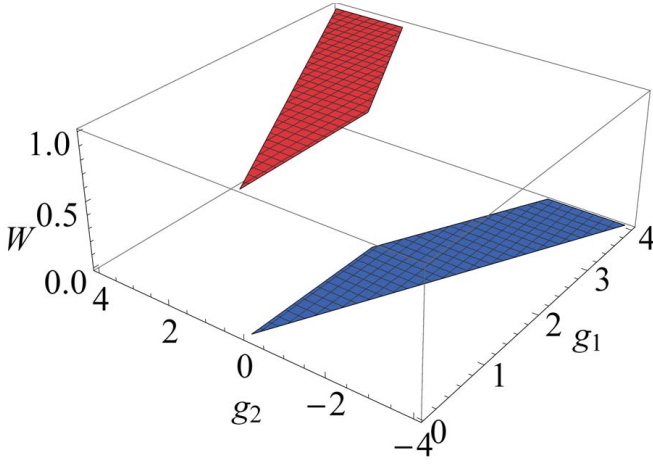


FIG. 7. Global Berry phase  $W$  for different  $g_1$  and  $g_2$  values in phases (II) and (III), which give complete bandgaps.  $W$  shows a discontinuous change:  $W = 1$  for  $g_2 > 0$  and  $W = 0$  for  $g_2 < 0$ , showing the topological transition at the gap closing,  $g_2 = 0$ . It can be said that  $\text{Im} W$  is numerically zero. The assigned differential step of wavenumber is  $\Delta k = 10^{-10}$ . Steps of calculation points in  $(g_1, g_2)$  are both 0.05.

the states are nondegenerate [84]. In addition, there is no constraint above in phase (III). Note that the global Berry phase avoids the difficulty of the  $4 \times 4$  Hamiltonian not giving off-block-diagonal  $Q$  matrices in a standard construction of the winding number [37].

We further notice that the eigenstates are  $4\pi$ -periodic in  $k$  by non-Hermiticity, as pointed out in Ref. 52. The loop of  $k$  for the states should therefore be two rounds of the first Brillouin zone, and the winding number should be an average of the Berry phase per round [85], namely,

$$W = \sum_s \frac{i}{2\pi} \left( \frac{1}{2} \int_{-\pi}^{2\pi} dk \langle \psi_{B,s} | \partial_k | \psi_{B,s} \rangle \right). \quad (\text{D1})$$

Although, we point out that the Berry connection in this case is  $2\pi$ -periodic and that the Berry phase accumulated in a single round of the Brillouin zone equals Eq. (D1). This is very probably because two EPs are always “encircled” in this gapped system.

### Appendix E: Detuned edge states

When  $g_1 = g_2$ , the behavior of the midgap edge states is different from those shown in the main text. For the system in phase (II), the real parts of their eigenfrequencies are slightly detuned from the single cavity resonance, i.e.  $\text{Re} \omega \neq 0$  [Fig. 8 (a)]. Their net gain  $\text{Im} \omega \neq 0$  is relatively small compared to systems with similar  $(g_1, g_2)$  satisfying  $g_1 \neq g_2$ . The mode patterns of these states show the intensity accumulation at both sides and their tails are extended to the center of the lattice [Fig. 8 (b)]. This real detuning decreases as  $g_1$  and  $g_2$  increase, and vanishes in phase (III).

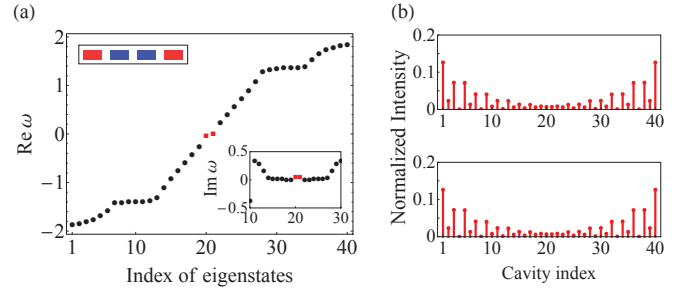


FIG. 8. Eigenstates for  $g_1 = g_2 = 0.5$ , of a 40 cavity system. (a) Sorted  $\text{Re} \omega$ . Upper left inset: schematic of the unit cell, with an imaginary potential of  $(0.5i, -0.5i, -0.5i, 0.5i)$ . Lower right inset:  $\text{Im} \omega$  for selected states. Squares: midgap states with  $\text{Re} \omega \neq 0$ . (b) Intensity distributions for the midgap states, with remaining weak couplings between the left-half and right-half edge modes.

Such peculiar properties stem from the interplay between the bulk antilinear symmetry and global mirror symmetry of the system. Because the eigenstates of the inversion operator  $\hat{P}$  must have even or odd parity with respect to the center of the lattice, the mirror symmetry  $[\hat{H}, \hat{P}] = 0$  localizes the midgap modes at both edges. Moreover, the exact antilinear symmetry of the Bloch eigenmodes around  $k = 0$  in phase (II) does not provide any sublattice mode localization, thus somewhat extended states are allowed in finite systems. Consequently, while the topological charge sweeps photons towards the edges, the right-half and left-half cavity clusters are not completely decoupled. The right and left cluster modes are in-phase and out-of-phase for the midgap states with lower and higher  $\text{Re} \omega$ , respectively. Meanwhile, we found that increasing the system cavity number, with retaining  $g_1$  and  $g_2$  values, barely affected the decay profile of the edge modes and hence suppressed the detuning (coupling between the edges). It means that these features above are finite-size effects, and edge states with  $\text{Re} \omega = 0$  are restored in the limit of the infinite system size [70].

### Appendix F: Bulk symmetry for nontrivial topology

The bulk system should have a symmetry that results in its nontrivial topology with the finite  $W$ . Here,  $\hat{H}(k)$  has a pseudo-anti-Hermiticity [37],  $\hat{H}(k) = -\hat{\eta} \hat{H}^\dagger(k) \hat{\eta}$ , where  $\hat{\eta} = \text{diag}(1, -1, 1, -1)$  in our system. The symmetry supports pairs of states with eigenfrequencies of  $\omega$  and  $-\omega^*$  via the duality relation. For our non-Hermitian system, this means  $\text{Re} \omega = 0$  (not always  $\text{Im} \omega = 0$ ), at  $k = 0$  under the existence of Dirac-like bands (topological transition points).

$\hat{H}(k)$  also has a chiral symmetry  $\hat{C}(k) \hat{H}(k) \hat{C}(k) = -\hat{H}(k)$  with  $\hat{C}(k) = \hat{S}(k) \hat{\eta}$  and  $\hat{S}(k) = \hat{\sigma}_x \otimes (\cos \frac{k}{2}) \hat{I}_2 + \hat{\sigma}_y \otimes (\sin \frac{k}{2}) \hat{I}_2$ , which guarantees couples of eigenvalues  $\pm \omega(k)$ . The system band structures, composed of four eigenstates, then satisfy both our chiral symme-

try and pseudo-anti-Hermiticity. Here, the pseudo-anti-Hermiticity can contribute to the topological protection in terms of  $\kappa$ ,  $g_1$  and  $g_2$ , because it is based on the purely local operator,  $\hat{\eta}$ . Meanwhile, the chiral symmetry is missing in our finite chains with termination at both sides, since  $\hat{C}(k)$  includes the translation operator  $\hat{S}(k)$ . Thus, the bulk chiral symmetry is irrelevant to the topological robustness of the edge states. Note that the bulk does not hold the particle-hole symmetry based on the local operator, which is valid for the finite lattice, because of the Bloch phase factor  $e^{\pm ika}$  in  $\hat{\mathcal{H}}(k)$  for the couplings between the unit cells.

$$\hat{\mathcal{H}} = \begin{pmatrix} \ddots & \kappa\xi_{\kappa,4l-4} & 0 & 0 & 0 & 0 \\ \kappa\xi_{\kappa,4l-4} & ig_1\xi_{g,4l-3} & \kappa\xi_{\kappa,4l-3} & 0 & 0 & 0 \\ 0 & \kappa\xi_{\kappa,4l-3} & -ig_2\xi_{g,4l-2} & \kappa\xi_{\kappa,4l-2} & 0 & 0 \\ 0 & 0 & \kappa\xi_{\kappa,4l-2} & -ig_1\xi_{g,4l-1} & \kappa\xi_{\kappa,4l-1} & 0 \\ 0 & 0 & 0 & \kappa\xi_{\kappa,4l-1} & ig_2\xi_{g,4l} & \kappa\xi_{\kappa,4l} \\ 0 & 0 & 0 & 0 & \kappa\xi_{\kappa,4l} & \ddots \end{pmatrix}, \quad (\text{G1})$$

where  $l$  is the unit index and all the parameters are real numbers. The fluctuation coefficients  $\{\xi_{\kappa,n}\}$  and  $\{\xi_{g,n}\}$  ( $n$ : cavity index) are all independent random numbers under Gaussian distribution with a mean of unity and a standard deviation of  $\sigma$ . Note that  $\hat{\mathcal{H}}$  is assumed to be a symmetric matrix due to the reciprocity of Hermitian cavity couplings.

Figure 9 shows example eigenstates for a disordered lattice ( $\sigma = 0.2$ ) in phase (II), based on the condition for Fig. 3 (b) in the main text. The midgap states with  $\text{Re}\omega = 0$  are obtained even with a variation of 20% in all the parameters [Fig. 9 (a)]. Furthermore, the edge localization of these modes is clearly maintained [Fig. 9 (b)]. This topological protection remains unless the bulk bandgap is effectively closed by the disorder. In an experimental system with controlled gain and loss, the non-Hermitian effect for dimerization will be stably kept in practice. Thus, variation in cavity couplings is the main factor in the symmetry preserving perturbation. It is also noteworthy that possible cavity frequency detuning in each cavity will be a more serious obstacle, because it breaks the symmetries and hence lifts the edge-state frequencies toward the bulk band edges [50].

As our final comments, we found that a similar structure to our system was included in an aperiodic lattice constructed according to Fibonacci Sequences [86]. However, such a lattice basically includes large detuning in

## Appendix G: Robustness of topological edge states

The edge states of the finite chains are topologically protected by the pseudo-anti-Hermiticity and equivalent particle-hole symmetry. Here, because these symmetries root on a local operator, no fluctuation in any of the parameters considered in the model can break them. Therefore, the edge states retain  $\text{Re}\omega = 0$  under such perturbation. To demonstrate this, we modify the lattice Hamiltonian as follows,

the real part of its refractive index profile for the design of its frequency response. Thus, its concept is clearly different from our work. Moreover, as described in Ref. 86, the defect states in such systems are induced not by a nontrivial photonic topology but by the PT phase transition. This can be seen by the fact that no edge state or defect state is reported in that system with the exact PT phase.

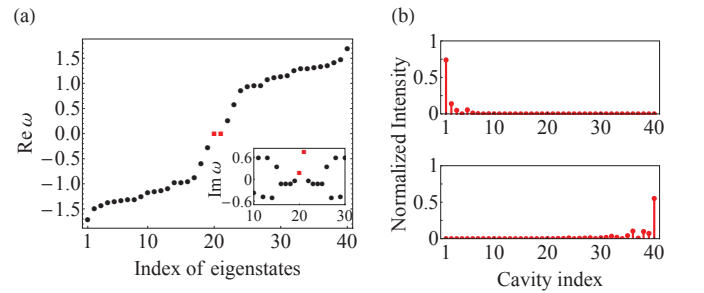


FIG. 9. Topological edge states under disorder in the cavity couplings, gain and loss.  $g_1 = 1$ ,  $g_2 = 0.5$  and  $\sigma = 0.2$ . (a) Sorted real parts of eigenvalues  $\text{Re}\omega$ . Squares: edge stages stabilized at  $\text{Re}\omega = 0$ . Inset: corresponding imaginary part  $\text{Im}\omega$ . (b) Intensity distributions of the edge states.

[1] A. Yariv and P. Yeh, *Photonics: optical electronics in modern communications*, 6th ed. (Oxford University

Press, New York, 2007).

[2] C. M. Bender and S. Boettcher, Phys. Rev. Lett. **80**, 5243



- (1998).
- [3] C. M. Bender, D. C. Brody, and H. F. Jones, *Phys. Rev. Lett.* **89**, 270401 (2002).
  - [4] K. G. Makris, R. El-Ganainy, D. N. Christodoulides, and Z. H. Musslimani, *Phys. Rev. Lett.* **100**, 103904 (2008).
  - [5] Z. H. Musslimani, K. G. Makris, R. El-Ganainy, and D. N. Christodoulides, *Phys. Rev. Lett.* **100**, 030402 (2008).
  - [6] S. Klaiman, U. Günther, and N. Moiseyev, *Phys. Rev. Lett.* **101**, 080402 (2008).
  - [7] A. Guo, G. J. Salamo, D. Duchesne, R. Morandotti, M. Volatier-Ravat, V. Aimez, G. A. Siviloglou, and D. N. Christodoulides, *Phys. Rev. Lett.* **103**, 093902 (2009).
  - [8] C. E. Rüter, K. G. Makris, R. El-Ganainy, D. N. Christodoulides, M. Segev, and D. Kip, *Nat. Phys.* **6**, 192 (2010).
  - [9] I. V. Barashenkov, S. V. Suchkov, A. A. Sukhorukov, S. V. Dmitriev, and Y. S. Kivshar, *Phys. Rev. A* **86**, 053809 (2012).
  - [10] A. Regensburger, C. Bersch, M.-A. Miri, G. Onishchukov, D. N. Christodoulides, and U. Peschel, *Nature* **488**, 167 (2012).
  - [11] S. Longhi, *Phys. Rev. Lett.* **103**, 123601 (2009).
  - [12] M. Wimmer, M.-A. Miri, D. Christodoulides, and U. Peschel, *Sci. Rep.* **5**, 17760 (2015).
  - [13] S. Longhi, *Opt. Lett.* **41**, 4518 (2016).
  - [14] Y. D. Chong, L. Ge, H. Cao, and A. D. Stone, *Phys. Rev. Lett.* **105**, 053901 (2010).
  - [15] S. Longhi, *Phys. Rev. A* **82**, 031801 (R) (2010).
  - [16] Y. Sun, W. Tan, H.-Q. Li, J. Li, and H. Chen, *Phys. Rev. Lett.* **112**, 143903 (2014).
  - [17] A. Szameit, M. C. Rechtsman, O. Bahat-Treidel, and M. Segev, *Phys. Rev. A* **84**, 021806 (R) (2011).
  - [18] K. Takata and M. Notomi, *Phys. Rev. Applied* **7**, 054023 (2017).
  - [19] Z. Lin, H. Ramezani, T. Eichelkraut, T. Kottos, H. Cao, and D. N. Christodoulides, *Phys. Rev. Lett.* **106**, 213901 (2011).
  - [20] L. Feng, Y.-L. Xu, W. S. Fegadolli, M.-H. Lu, J. E. B. Oliveira, V. R. Almeida, Y.-F. Chen, and A. Scherer, *Nat. Mater.* **12**, 108 (2013).
  - [21] H. Ramezani, H.-K. Li, Y. Wang, and X. Zhang, *Phys. Rev. Lett.* **113**, 263905 (2014).
  - [22] B. Peng, S. K. Özdemir, F. Lei, F. Monifi, M. Gianfreda, G. L. Long, S. Fan, F. Nori, C. M. Bender, and L. Yang, *Nat. Phys.* **10**, 394 (2014).
  - [23] L. Chang, X. Jiang, S. Hua, C. Yang, J. Wen, L. Jiang, G. Li, G. Wang, and M. Xiao, *Nat. Photonics* **8**, 524 (2014).
  - [24] L. Feng, Z. J. Wong, R.-M. Ma, Y. Wang, and X. Zhang, *Science* **346**, 972 (2014).
  - [25] H. Hodaei, M.-A. Miri, M. Heinrich, D. N. Christodoulides, and M. Khajavikhan, *Science* **346**, 975 (2014).
  - [26] Z. Gao, S. T. M. Fryslie, B. J. Thompson, P. S. Carney, and K. D. Choquette, *Optica* **4**, 323 (2017).
  - [27] L. Feng, R. El-Ganainy, and L. Ge, *Nat. Photonics* **11**, 752 (2017).
  - [28] R. El-Ganainy, K. G. Makris, M. Khajavikhan, Z. H. Musslimani, S. Rotter, and D. N. Christodoulides, *Nat. Phys.* **14**, 11 (2018).
  - [29] F. D. M. Haldane and S. Raghu, *Phys. Rev. Lett.* **100**, 013904 (2008).
  - [30] L. Lu, J. D. Joannopoulos, and M. Soljačić, *Nat. Photonics* **8**, 821 (2014).
  - [31] L. Lu, J. D. Joannopoulos, and M. Soljačić, *Nat. Phys.* **12**, 626 (2016).
  - [32] K. v. Klitzing, G. Dorda, and M. Pepper, *Phys. Rev. Lett.* **45**, 494 (1980).
  - [33] D. J. Thouless, M. Kohmoto, M. P. Nightingale, and M. den Nijs, *Phys. Rev. Lett.* **49**, 405 (1982).
  - [34] C. L. Kane and E. J. Mele, *Phys. Rev. Lett.* **95**, 146802 (2005).
  - [35] M. Z. Hasan and C. L. Kane, *Rev. Mod. Phys.* **82**, 3045 (2010).
  - [36] M. Sato, K. Hasebe, K. Esaki, and M. Kohmoto, *Prog. Theor. Phys.* **127**, 937 (2012).
  - [37] K. Esaki, M. Sato, K. Hasebe, and M. Kohmoto, *Phys. Rev. B* **84**, 205128 (2011).
  - [38] Y. C. Hu and T. L. Hughes, *Phys. Rev. B* **84**, 153101 (2011).
  - [39] C. Yu, *Phys. Lett. A* **379**, 1213 (2015).
  - [40] C. Yu, *Eur. Phys. J. D* **69**, 184 (2015).
  - [41] H. Schomerus, *Opt. Lett.* **38**, 1912 (2013).
  - [42] W. P. Su, J. R. Schrieffer, and A. J. Heeger, *Phys. Rev. Lett.* **42**, 1698 (1979).
  - [43] C. Poli, M. Bellec, U. Kuhl, F. Mortessagne, and H. Schomerus, *Nat. Commun.* **6**, 6710 (2015).
  - [44] J. M. Zeuner, M. C. Rechtsman, Y. Plotnik, Y. Lumer, S. Nolte, M. S. Rudner, M. Segev, and A. Szameit, *Phys. Rev. Lett.* **115**, 040402 (2015).
  - [45] S. Weimann, M. Kremer, Y. Plotnik, Y. Lumer, S. Nolte, K. G. Makris, M. Segev, M. C. Rechtsman, and A. Szameit, *Nat. Mater.* **16**, 433 (2017).
  - [46] P. St-Jean, V. Goblot, E. Galopin, A. Lemaître, T. Ozawa, L. L. Gratiet, I. Sagnes, J. Bloch, and A. Amo, *Nat. Photonics* **11**, 651 (2017).
  - [47] M. Parto, S. Wittek, H. Hodaei, G. Harari, M. A. Bandres, J. Ren, M. C. Rechtsman, M. Segev, D. N. Christodoulides, and M. Khajavikhan, *arXiv:1709.00523* (2017).
  - [48] H. Zhao, P. Miao, M. H. Teimourpour, S. Malzard, R. El-Ganainy, H. Schomerus, and L. Feng, *arXiv:1709.02747* (2017).
  - [49] B. Bahari, A. Ndao, F. Vallini, A. E. Amili, Y. Fainman, and B. Kanté, *Science* (2017), 10.1126/science.aao4551.
  - [50] N. Malkova, I. Hromada, X. Wang, G. Bryant, and Z. Chen, *Opt. Lett.* **34**, 1633 (2009).
  - [51] S. Aubry and G. André, *Ann. Isr. Phys. Soc.* **3**, 133 (1980).
  - [52] T. E. Lee, *Phys. Rev. Lett.* **116**, 133903 (2016).
  - [53] G. Q. Liang and Y. D. Chong, *Phys. Rev. Lett.* **110**, 203904 (2013).
  - [54] H. Kogelnik and C. V. Shank, *J. Appl. Phys.* **43**, 2327 (1972).
  - [55] S. Malzard, C. Poli, and H. Schomerus, *Phys. Rev. Lett.* **115**, 200402 (2015).
  - [56] H. Zhao, S. Longhi, and L. Feng, *Sci. Rep.* **5**, 17022 (2015).
  - [57] D. Leykam, K. Y. Bliokh, C. Huang, Y. D. Chong, and F. Nori, *Phys. Rev. Lett.* **118**, 040401 (2017).
  - [58] H. Hodaei, A. U. Hassan, S. Wittek, H. Garcia-Gracia, R. El-Ganainy, D. N. Christodoulides, and M. Khajavikhan, *Nature* **548**, 187 (2017).
  - [59] N. B. Nguyen, S. A. Maier, M. Hong, and R. F. Oulton, *New J. Phys.* **18**, 125012 (2016).
  - [60] See Supplementary Materials for describing the system

- gapless phases, bandgap opening, effective decoupling, topological number, possible finite size effects, bulk symmetry and robustness of the topological edge states.
- [61] A. Mostafazadeh, *J. Math. Phys.* **43**, 205 (2002).
  - [62] A. Mostafazadeh, *J. Math. Phys.* **43**, 3944 (2002).
  - [63] S.-D. Liang and G.-Y. Huang, *Phys. Rev. A* **87**, 012118 (2013).
  - [64] J. Zak, *Phys. Rev. Lett.* **62**, 2747 (1989).
  - [65] Y. Hatsugai, *J. Phys. Soc. Jpn.* **73**, 2604 (2004).
  - [66] F. Keck, H. J. Korsch, and S. Mossmann, *J. Phys. A: Math. Gen.* **36**, 2125 (2003).
  - [67] S. Ryu, A. P. Schnyder, A. Furusaki, and A. W. W. Ludwig, *New J. Phys.* **12**, 065010 (2010).
  - [68] D. I. Pikulin and Y. V. Nazarov, *JETP Lett.* **94**, 693 (2012).
  - [69] D. I. Pikulin and Y. V. Nazarov, *Phys. Rev. B* **87**, 235421 (2013).
  - [70] S. Ryu and Y. Hatsugai, *Phys. Rev. Lett.* **89**, 077002 (2002).
  - [71] A. Blanco-Redondo, I. Andonegui, M. J. Collins, G. Harari, Y. Lumer, M. C. Rechtsman, B. J. Eggleton, and M. Segev, *Phys. Rev. Lett.* **116**, 163901 (2016).
  - [72] H. Jing, S. K. Özdemir, X.-Y. Lü, J. Zhang, L. Yang, and F. Nori, *Phys. Rev. Lett.* **113**, 053604 (2014).
  - [73] X. Zhu, H. Ramezani, C. Shi, J. Zhu, and X. Zhang, *Phys. Rev. X* **4**, 031042 (2014).
  - [74] X.-Y. Lü, H. Jing, J.-Y. Ma, and Y. Wu, *Phys. Rev. Lett.* **114**, 253601 (2015).
  - [75] J. Schindler, A. Li, M. C. Zheng, F. M. Ellis, and T. Kotlos, *Phys. Rev. A* **84**, 040101 (2011).
  - [76] B. Lv, J. Fu, B. Wu, R. Li, Q. Zeng, X. Yin, Q. Wu, L. Gao, W. Chen, Z. Wang, Z. Liang, A. Li, and R. Ma, *Sci. Rep.* **7**, 40575 (2017).
  - [77] A. A. Burkov and L. Balents, *Phys. Rev. Lett.* **107**, 127205 (2011).
  - [78] M. C. Rechtsman, J. M. Zeuner, Y. Plotnik, Y. Lumer, D. Podolsky, F. Dreisow, S. Nolte, M. Segev, and A. Szameit, *Nature* **496**, 196 (2013).
  - [79] J. Doppler, A. A. Mailybaev, J. Böhm, U. Kuhl, A. Girschik, F. Libisch, T. J. Milburn, P. Rabl, N. Moiseyev, and S. Rotter, *Nature* **537**, 76 (2016).
  - [80] A. U. Hassan, B. Zhen, M. Soljačić, M. Khajavikhan, and D. N. Christodoulides, *Phys. Rev. Lett.* **118**, 093002 (2017).
  - [81] B. Zhen, C. W. Hsu, Y. Igarashi, L. Lu, I. Kaminer, A. Pick, S.-L. Chua, J. D. Joannopoulos, and M. Soljačić, *Nature* **525**, 354 (2015).
  - [82] M. Berry, *Czech. J. Phys.* **54**, 1039 (2004).
  - [83] W. D. Heiss, *J. Phys. A: Math. Theor.* **45**, 444016 (2012).
  - [84] F. H. M. Faisal and J. V. Moloney, *J. Phys. B* **14**, 3603 (1981).
  - [85] T. E. Lee, “Reply to comment on “Anomalous Edge State in a Non-Hermitian Lattice”,” [arXiv:1611.00355](https://arxiv.org/abs/1611.00355).
  - [86] X.-F. Zhu, *Opt. Express* **23**, 22274 (2015).